Eur. Phys. J. A **30**, 519–529 (2006)
DOI 10.1140/epja/i2006-10147-0

THE EUROPEAN PHYSICAL JOURNAL A

Improved BCS-type pairing for the relativistic mean-field theory

Hongfei Zhang[1,2], Soojae Im[1], Junqing Li[1,3,5,a], Wei Zuo[1,3,5], Zhongyu Ma[3,4], Baoqiu Chen[3,4], and W. Scheid[5]

[1] Institute of Modern Physics, Chinese Academy of Science, Lanzhou 730000, PRC
[2] School of Nuclear Science and Technology, Lanzhou University, Lanzhou 730000, PRC
[3] Research Center of Nuclear Theory of the Laboratory of Heavy Ion Accelerator of Lanzhou, Lanzhou 730000, PRC
[4] China Institute of Atomic Energy, Beijing 102413, PRC
[5] Institut für Theoretische Physik, Justus-Liebig-Universität, Giessen 35392, Germany

Received: 7 February 2006 / Revised: 6 November 2006 /
Published online: 14 December 2006 –
Communicated by G. Orlandini

Abstract. A density-dependent δ interaction (DDDI) is proposed in the formalism of BCS-type pairing correlations for exotic nuclei whose Fermi surfaces are close to the threshold of the unbound state. It provides the possibility to pick up those states whose wave functions are concentrated in the nuclear region by making the pairing matrix elements state dependent. On this basis, the energy level distributions, occupations, and ground-state properties are self-consistently studied in the RMF theory with deformation. Calculations are performed for the Sr isotopic chain. A good description of the total energy per nucleon, deformations, two-neutron separation energies and isotope shift from the proton drip line to the neutron drip line is found. Especially, by comparing the single-particle structure from the DDDI pairing interaction with that from the constant pairing interaction for a very neutron-rich nucleus it is demonstrated that the DDDI pairing method improves the treatment of the pairing in the continuum.

PACS. 21.30.-x Nuclear forces – 21.10.Dr Binding energies and masses – 21.10.Pc Single-particle levels and strength functions – 21.10.Gv Mass and neutron distributions

1 Introduction

The newly constructed radioactive beam facilities in the world have provided an opportunity to access exotic nuclei, and furthermore superheavy elements till $Z = 116$, and $Z = 118$ have been synthesized in the lab. All these new achievements are very exciting, however, the overall understanding of the properties of nuclei far from the β-stable valley and at the heaviest end of the periodic table by current existing theories is still far from complete. The recent developments showed that the relativistic mean-field (RMF) theory can describe the bulk properties of nuclei at the β-stable valley, as well as nuclei far from the β-stable line [1–6] and superheavy nuclei [7–10]. However, the properties of exotic nuclei near the drip lines show rather different features from those of stable nuclei. New types of isotopic-dependent interactions among nucleons appear and may become dominant. Nuclear densities, sizes, level fillings, and nuclear excitations of exotic nuclei may be quite different from those which we have encountered so far. The most distinct phenomena for nuclei near the drip line are the weak binding and the appearance of the resonant states in the continuum, which are also the common phenomena for superheavy nuclei since they are usually neutron deficient [11]. Their Fermi surfaces are thus close to the positive level and there are some protons distributed in positive levels. The direct consequence is that the constant pairing component of the effective interaction can no longer be treated as a residual interaction, since the constant pairing interaction (CPI) of the BCS method becomes comparable to the mean field [12,13].

It is our desire to obtain a model valid for all nuclei, including unstable ones, from the proton drip line to the neutron drip line. In a realistic description for finite nuclei, the deformation and pairing correlations must be included. Pairing correlations are very important for the ground-state properties of open-shell nuclei, and are especially crucial for a quantitative understanding of the size and deformation of heavy nuclei. Different methods have been developed in refs. [4,14,15] and references therein to treat the pairing correlation self-consistently. A simple and commonly used method to deal with the pairing interaction is the Bardeen-Cooper-Schrieffer (BCS) theory, which considers the pairing interaction as a perturbation. The conventional BCS method with the constant pairing interaction works well except in the case in which the Fermi surface is close to the unbound

[a] e-mail: jqli@lzb.ac.cn

threshold [13]. Dobaczewski *et al.* have shown that the BCS approximation breaks down, if one has finite occupation probabilities for levels in the continuum, and pointed out that the roles of finite range and of density dependence are two important points for the microscopic study of the pairing interaction [14]. The finite-range effect can be modeled by an explicit velocity dependence. Early calculations [16,17] for nuclear matter predicted a very weak $^1S_0$ pairing at the saturation point ($k_f = 1.35\,\mathrm{fm}^{-1}$), so it was concluded that strong pairing correlations in finite nuclei had to be due to interactions at the nuclear surface. The surface delta interaction (SDI) was thus used to deal with the problem [18,19], however, the density-dependent delta interaction (DDDI) is a more realistic density-dependent pairing force [20]. In this work, we include the DDDI into the deformed RMF theory to calculate the pairing matrix element for the proton and neutron orbitals of even Sr isotopes.

The self-consistent RMF theory was first extended by Greiner *et al.* [21], Price *et al.* [22], and Gambhir *et al.* [23] to treat deformed nuclei. In Gambhir's work, the nucleon wave functions and the meson fields are expanded in terms of the harmonic-oscillator wave functions. We employ this method for the mean-field part and improve the BCS part with a density-dependent delta-function interaction. The use of the nuclear wave function, particularly the overlap between occupied and unoccupied states, is resolved reasonably, which allows us to take into account states in the continuum whose wave functions are concentrated in the nuclear region.

Sandulescu [24] *et al.* have presented a simple scheme for taking into account the resonant continuum coupling in the relativistic mean field - BCS calculations. In this scheme, applied before in nonrelativistic calculations, the effect of the resonant continuum on pairing correlations is introduced through the scattering wave functions located in the region of the resonant states. These states are found by solving the relativistic mean-field equations with scattering-type boundary conditions for the continuum spectrum. It would be interesting to distinguish resonant states from the continuum states, and to study the properties of the exotic nuclei including resonance continuum states.

The paper is organized as follows. In sect. 2, we present the RMF formalism with deformation and pairing. In sect. 3, we apply the method to Sr isotopes from the proton drip line to the neutron drip line. We compare our calculated results with those obtained with the finite-range drop model (FRDM) [25] and the known experimental values. In sect. 4, we summarize the presented results.

2 RMF with deformation and pairing

We present here the formulation of the RMF theory with deformation and pairing correlations. The starting point for the relativistic model is the Lagrange density $\mathcal{L}$ [4]:

$$\begin{aligned}\mathcal{L} = {} & \bar{\psi}(i\gamma^\mu\partial_\mu - M)\psi + \frac{1}{2}\partial_\mu\sigma\partial^\mu\sigma - \frac{1}{2}m_\sigma^2\sigma^2 \\ & -\frac{1}{3}g_2\sigma^3 - \frac{1}{4}g_3\sigma^4 - g_\sigma\bar{\psi}\sigma\psi \\ & -\frac{1}{4}\Omega_{\mu\nu}\Omega^{\mu\nu} + \frac{1}{2}m_\omega^2\omega_\mu\omega^\mu - g_\omega\bar{\psi}\gamma^\mu\psi\omega_\mu \\ & -\frac{1}{4}R^a{}_{\mu\nu}R^{a\mu\nu} + \frac{1}{2}m_\rho^2\rho_\mu^a\rho^{a\mu} - g_\rho\bar{\psi}\gamma_\mu\tau^a\psi\rho^{\mu a} \\ & -\frac{1}{4}F_{\mu\nu}F^{\mu\nu} - e\bar{\psi}\gamma_\mu\frac{1-\tau_3}{2}A^\mu\psi,\end{aligned} \tag{1}$$

The nucleon field ψ having mass M interacts with σ-, ω-, ρ-meson fields: σ, ω_μ, ρ_μ and the photon field A_μ. The self-coupling terms with coupling constants g_2 and g_3 for the σ-meson are introduced [26] to improve the compressibility of nuclear matter. The isospin dependence of the nuclear interaction is provided by the isovector ρ-meson. The field tensors of the vector mesons and of the electromagnetic field take the following forms:

$$\begin{cases}\Omega_{\mu\nu} = \partial_\mu\omega_\nu - \partial_\nu\omega_\mu, \\ R^a_{\mu\nu} = \partial_\mu\rho^a_\nu - \partial_\nu\rho^a_\mu - 2g_\rho\epsilon^{abc}\rho^b_\mu\rho^c_\nu, \\ F_{\mu\nu} = \partial_\mu A_\nu - \partial_\nu A_\mu,\end{cases} \tag{2}$$

where the symbols have their usual meanings.

The classical variational principle leads to the Dirac equation

$$\left[-i\alpha\nabla + V(\mathbf{r}) + \beta\left(M + S(\mathbf{r})\right)\right]\psi_i = \epsilon_i\psi_i \tag{3}$$

for the nucleon spinors and the Klein-Gordon equations

$$\begin{cases}\{-\Delta + m_\sigma^2\}\sigma(\mathbf{r}) = -g_\sigma\rho_s(\mathbf{r}) - g_2\sigma^2(\mathbf{r}) - g_3\sigma^3(\mathbf{r}), \\ \{-\Delta + m_\omega^2\}\omega^\mu(\mathbf{r}) = g_\omega j^\mu(\mathbf{r}) + g_4\omega_\mu^2(\mathbf{r})\omega^\mu(\mathbf{r}), \\ \{-\Delta + m_\rho^2\}\rho^{a\mu}(\mathbf{r}) = g_\rho j^{a\mu}(\mathbf{r}), \\ -\Delta A^\mu(\mathbf{r}) = e j_p^\mu(\mathbf{r})\end{cases} \tag{4}$$

for the meson and the electromagnetic fields. Here, $V(\mathbf{r})$ is the vector potential

$$V(\mathbf{r}) = g_\omega\gamma^\mu\omega_\mu(\mathbf{r}) + g_\rho\tau^a\gamma^\mu\rho^a_\mu(\mathbf{r}) + e\frac{1-\tau_3}{2}\gamma^\mu A_\mu(\mathbf{r}), \tag{5}$$

and $S(\mathbf{r})$ the scalar potential

$$S(\mathbf{r}) = g_\sigma\sigma(\mathbf{r}). \tag{6}$$

For the mean-field approximation, the scalar nuclear density and the various current densities are given with nucleon spinors and provide the corresponding source terms in eq. (4):

$$\begin{cases}\rho_s(\mathbf{r}) = \sum_{i=1}^{A}\bar{\psi}_i\,\psi_i, \\ j^\mu(\mathbf{r}) = \sum_{i=1}^{A}\bar{\psi}_i\gamma^\mu\psi_i, \\ j^{a\mu}(\mathbf{r}) = \sum_{i=1}^{A}\bar{\psi}_i\gamma^\mu\tau^a\psi_i, \\ j_p^\mu(\mathbf{r}) = \sum_{i=1}^{A}\bar{\psi}_i\gamma^\mu\frac{1-\tau_3}{2}\psi_i.\end{cases} \tag{7}$$

Here, the summations are taken over the Fermi sea nucleons only. It should be noted that as usual, the present approach ignores the contribution of negative-energy states (*i.e.* no-sea approximation) which implies that the vacuum is not polarized. The π-meson does not contribute in the present relativistic mean-field (Hartree) approximation because of its pseudoscalar nature. The coupled equations (3) and (4) are nonlinear quantum field equations, and their exact solutions are very complicated. For this reason, the mean-field approximation is generally used; *i.e.*, the meson field operators in eq. (3) are replaced by their expectation values. In this treatment, nucleons are considered to move independently in the classical meson fields. The coupled equations are solved self-consistently by iteration.

The symmetries of the system simplify the calculations considerably. In all the systems considered in this work, there exists the time reversal symmetry, so there are no currents in the nucleus and therefore the spatial vector components of ω^μ, $\rho^{a\mu}$ and A^μ vanish. This leaves only the time-like components, ω^0, ρ^{a0} and A^0. Charge conservation guarantees that only the 3-component of the isovector ρ^{00} survives.

2.1 The axially symmetric case

The RMF theory was extended by W. Greiner *et al.* [21] and Gambhir *et al.* [23] to treat deformed nuclei with axially symmetric shapes. In the next step, we deduce the pairing matrix. In order to clear the notations used, we give a brief review of the RMF method for axially deformed nuclei.

Many deformed nuclei can be described with axially symmetric shapes. In this case, the rotational symmetry is lost, and therefore the total angular momentum, j, is no longer a good quantum number. However, the densities are still invariant with respect to the rotation about the symmetry axis, which is assumed to be the z-axis in the following. It is then useful to work with cylindrical coordinates: $x = r_\perp \cos\varphi$, $y = r_\perp \sin\varphi$ and z. For such nuclei, the Dirac equation can be reduced to a coupled set of partial differential equations in the two variables z and $r_\perp$. In particular, the spinor ψ_i with the index i is now characterized by the quantum numbers Ω_i, π_i and t_i, where $\Omega_i = m_{l_i} + m_{s_i}$ is the eigenvalue of the Z-component of the angular-momentum operator J_z, π_i is the parity and t_i is the isospin. The spinor can be written in the form

$$\psi_i(\mathbf{r},t) = \begin{pmatrix} f_i(\mathbf{r}) \\ ig_i(\mathbf{r}) \end{pmatrix} = \frac{1}{\sqrt{2\pi}} \begin{pmatrix} f_i^+(z,r_\perp)e^{i(\Omega_i-1/2)\varphi} \\ f_i^-(z,r_\perp)e^{i(\Omega_i+1/2)\varphi} \\ ig_i^+(z,r_\perp)e^{i(\Omega_i-1/2)\varphi} \\ ig_i^-(z,r_\perp)e^{i(\Omega_i+1/2)\varphi} \end{pmatrix} \chi_{t_i}(t). \tag{8}$$

The four components $f_i^\pm(z,r_\perp)$ and $g_i^\pm(z,r_\perp)$ obey the coupled Dirac equations. For each solution with positive Ω_i, ψ_i, we have the time-reversed solution with the same energy, $\psi_{\bar{i}} = T\psi_i$, with the time reversal operator $T = -i\sigma_y K$ (K being the complex conjugation). For nuclei with time reversal symmetry, the contributions to the densities of the two time reversed states, i and $\bar{i}$, are identical. Therefore, we find the densities

$$\rho_{s,v} = 2\sum_{i>0} \left(\left(|f_i^+|^2 + |f_i^-|^2\right) \mp \left(|g_i^+|^2 + |g_i^-|^2\right) \right) \tag{9}$$

and, in a similar way, ρ_c and ρ_3. (Here ρ_3 is the third component of the ρ-meson density, which is the only remained component due to charge conservation.) The sum here runs over only states with positive Ω_i. These densities serve as sources for the fields $\phi = \sigma, \omega^0, \rho^{00}$ and A^0, which are determined by the Klein-Gordon equations in cylindrical coordinates.

To solve the RMF equations, the basis expansion method is used. We closely follow the detailed presentations and notations of ref. [27]. For the axially symmetric case, the spinors $f_i^\pm$ and $g_i^\pm$ in eq. (8) are expanded in terms of the eigenfunctions of a deformed axially symmetric oscillator potential,

$$V_{osc}(z,r_\perp) = \frac{1}{2}M\omega_z^2 z^2 + \frac{1}{2}M\omega_\perp^2 r_\perp^2. \tag{10}$$

Then, by imposing the volume conservation, the two oscillator frequencies $\omega_\perp$ and ω_z can be expressed in terms of a deformation parameter, β_0: $\omega_z = \omega_0 \exp(-\sqrt{\frac{5}{4\pi}}\beta_0)$ and $\omega_\perp = \omega_0 \exp(+\frac{1}{2}\sqrt{\frac{5}{4\pi}}\beta_0)$.

The basis is now determined by the two constants ω_0 and β_0. The eigenfunctions of the deformed harmonic-oscillator potential are characterized by the quantum numbers, $|\alpha\rangle = |n_z, n_r, m_l, m_s\rangle$, where m_l and m_s are the components of the orbital angular momentum and of the spin along the symmetry axis, respectively. The eigenvalue of J_z, which is a conserved quantity in these calculations, is $\Omega = m_l + m_s$. The parity is given by $\pi = (-)^{n_z+m_l}$.

The eigenfunctions of the deformed harmonic oscillator can be written explicitly as

$$\Phi_\alpha(z,r_\perp,\varphi,s,t) = \phi_{n_z}(z)\phi_{n_r}^{m_l}(r_\perp)\frac{1}{\sqrt{2\pi}}e^{im_l\varphi}\chi_{m_s}(s)\chi_{t_\alpha}(t), \tag{11}$$

with

$$\begin{aligned} \phi_{n_z}(z) &= \frac{N_{n_z}}{\sqrt{b_z}} H_{n_z}(\zeta) e^{-\zeta^2/2}, \\ \phi_{n_r}^{m_l}(r_\perp) &= \sqrt{2}\frac{N_{n_r}^{m_l}}{b_\perp}\eta^{m_l/2} L_{n_r}^{m_l}(\eta) e^{-\eta/2}, \end{aligned} \tag{12}$$

where $\zeta = z/b_z$ and $\eta = r_\perp^2/b_\perp^2$. The polynomials $H_n(\zeta)$ and $L_n^m(\eta)$ are the Hermite polynomials and the associated Laguerre polynomials, respectively, as defined in ref. [28]. The quantities N_{n_z} and $N_{n_r}^{m_l}$ are normalization constants.

The spinors $f_i^{\pm}$ and $g_i^{\pm}$ in eq. (8) are explicitly given by the following relations:

$$\begin{cases} f_i^+(z,r_\perp) = \sum_\alpha^{\alpha_{max}} f_\alpha^{(i)} \phi_{n_z}(z) \phi_{n_r}^{(\Omega-1/2)}(r_\perp), \\ f_i^-(z,r_\perp) = \sum_\alpha^{\alpha_{max}} f_\alpha^{(i)} \phi_{n_z}(z) \phi_{n_r}^{(\Omega+1/2)}(r_\perp), \\ g_i^+(z,r_\perp) = \sum_\beta^{\beta_{max}} g_\beta^{(i)} \phi_{n_z}(z) \phi_{n_r}^{(\Omega-1/2)}(r_\perp), \\ g_i^-(z,r_\perp) = \sum_\beta^{\beta_{max}} g_\beta^{(i)} \phi_{n_z}(z) \phi_{n_r}^{(\Omega+1/2)}(r_\perp). \end{cases} \tag{13}$$

The quantum numbers α_{max} and β_{max} are chosen in such a way that the corresponding major quantum numbers $N = n_z + 2n_\rho + m_l$ are not larger than $N_f + 1$ for the expansion of the small components and not larger than N_f for the expansion of the large components, where N_f is the maximum major shell number we are using here, and which is 12.

2.2 Pairing with the density-dependent delta-function interaction

Based on the single-particle spectrum calculated with the RMF method described above, we carry out a state-dependent BCS calculation [29,30]. In order to improve the calculation on the pairing correction, we introduce the DDDI:

$$V = -V_0 \left[1 - \left(\frac{\rho(\mathbf{r})}{\rho_0}\right)^\gamma\right] \delta(\mathbf{r}_1 - \mathbf{r}_2), \tag{14}$$

where $\rho(\mathbf{r})$ is the isoscalar nucleon density, $\gamma = 1$ and $\rho_0 = 0.16\,\mathrm{fm}^{-3}$ (the saturation density of symmetric nuclear matter), and actually only its $S = 0$ part of this pairing interaction form is used here. As in the seniority pairing calculations, we consider only spin-singlet neutron-neutron, and proton-proton pairing. For either neutrons or protons, the pairing matrix elements may be written as [19]

$$\bar{V}_{i\bar{i}j\bar{j}} = \langle i\bar{i}|V|j\bar{j}\rangle - \langle i\bar{i}|V|\bar{j}j\rangle = -V_0 \int \mathrm{d}^3r \left[1 - \left(\frac{\rho(\mathbf{r})}{\rho_0}\right)^\gamma\right] \times \left(\psi_i^\dagger \psi_{\bar{i}}^\dagger \psi_j \psi_{\bar{j}} - \psi_i^\dagger \psi_{\bar{i}}^\dagger \psi_{\bar{j}} \psi_j\right). \tag{15}$$

It is necessary to prevent the unrealistic pairing of highly excited states, and to confine the region of influence of the pairing potential to the vicinity of the Fermi surface. As discussed in ref. [31], this is accomplished by defining the pairing contribution E_{pair} to the total energy as

$$E_{pair} = \sum f_i u_i v_i f_j u_j v_j V_{i\bar{i}j\bar{j}}, \tag{16}$$

where u_i and v_i are the BCS factors, and the cutoff factors f_i are taken as

$$f_i^2 = \left(1 + \exp\left(\frac{\varepsilon_i - \lambda - \Delta\varepsilon}{\mu}\right)\right)^{-1}, \tag{17}$$

where $\Delta\varepsilon = 5\,\mathrm{MeV}$ and $\mu = 0.5\,\mathrm{MeV}$ [31] are choosen. A wider pairing window will cause the failure of the convergence of some nuclei. However, the smooth cutoff factor of eq. (17) actually leads to including more states around the vicinity of the Fermi surface, the considered states are not sharply cut off within 5 MeV about the Fermi surface. With this definition of the pairing energy, the state-dependent energy gaps Δ_i are the solution of the equations

$$\Delta_i = -\frac{1}{2} \sum \frac{f_j \bar{V}_{i\bar{i}j\bar{j}} \Delta_j}{\sqrt{(\varepsilon_j - \lambda)^2 + f_j^2 \Delta_j^2}}, \tag{18}$$

where ε_j is the single-particle energy and λ is the Fermi energy. The pairing energy and occupation probabilities may be written as

$$E_{pair} = -\frac{1}{2} \sum \frac{f_i^2 \Delta_i^2}{\sqrt{(\varepsilon_i - \lambda)^2 + f_i^2 \Delta_i^2}}, \tag{19}$$

$$v_i^2 = \frac{1}{2}\left[1 - \frac{\varepsilon_i - \lambda}{\sqrt{(\varepsilon_i - \lambda)^2 + f_i^2 \Delta_i^2}}\right], \tag{20}$$

where the particle number condition is given by $2\sum v_i^2 = N$. Equations (3) and (4), the gap equations (18), and the total particle number condition N for a given nucleus are solved self-consistently by iteration.

3 The calculation of ground-state properties

We apply the RMF theory with the improved BCS-type pairing to the ground-state properties of axially deformed even Sr isotopes including the nuclei far from the stability line. The calculations have been carried out using the parameter set NL-SH, which has been used to reproduce the experimental neutron radius, and deformation for exotic nuclei on both sides of the stability line [32]. Nuclear spinors and meson fields are expanded in an axially symmetric harmonic-oscillator basis with $\hbar\omega_0 = 41A^{-1/3}\,\mathrm{MeV}$. The major shell is chosen as $N_f = 12$ and $N_b = 12$ for nucleons and mesons, respectively, as described in ref. [27]. For the improved pairing interaction, we take the strength of the delta-function interaction as $850\,\mathrm{MeV\,fm^3}$ for neutrons and protons, which can give reasonable pairing gaps of the Sr isotopes. In order to show the improvement of the density-dependent pairing interaction, we also do the calculation for Sr isotopes with the relativistic mean-field theory with the constant pairing interaction (RMF(CPI)). In the RMF(CPI) calculation, we used $G_n = 15.0\,\mathrm{MeV}/A$ and $G_p = 20.0\,\mathrm{MeV}/A$, where A is the mass number, and the pairing window $\varepsilon_i - \lambda \leq 2(41A^{-1/3})\,\mathrm{MeV}$ [23]. Here, we used different pairing strengths, G_p and G_n, for protons and neutrons in order to obtain the same total energies as those obtained by the RMF(DDDI) for Sr isotopes.

3.1 The pairing gap

By using the improved BCS-type DDDI pairing in the RMF theory in deformed nuclei, the pairing gaps both

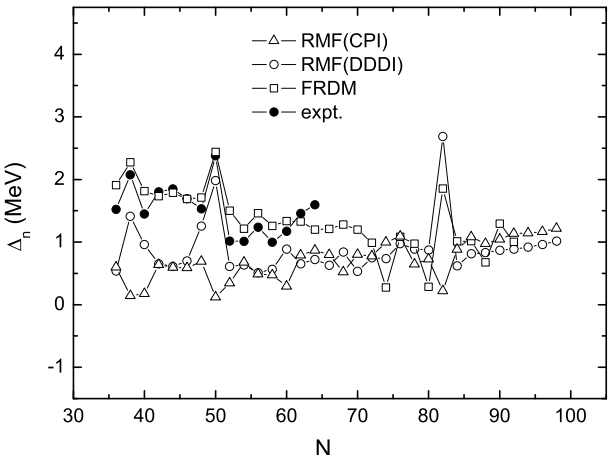

Fig. 1. The neutron pairing gap for the Sr isotope chain against the neutron number N.

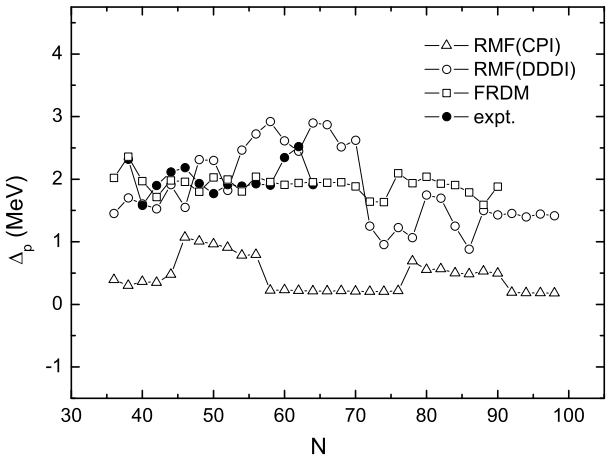

Fig. 2. The proton pairing gap for the Sr isotope chain against the neutron number N.

for neutron and proton are determined in a self-consistent way along the Sr isotope chain. The gaps are evaluated by taking the average [33] of the amplitudes v_k and u_k:

$$\langle uv\Delta\rangle = \frac{\sum_{k\in\Omega_q} f_k u_k v_k \Delta_k}{\sum_{k\in\Omega_q} f_k u_k v_k}\,, \tag{21}$$

where $q \in \{p, n\}$, and the smooth energy-dependent cutoff weights are shown in eq. (17).

The neutron and proton pairing gaps are shown in fig. 1 and fig. 2 as a function of the neutron number of Sr isotope nuclei, respectively; the results from RMF(CPI), the finite-range drop model (FRDM) [25] and the experimental data are also shown for comparison. The results of Δ calculated by RMF(CPI) are more deviated from the experimental data and from those by FRDM, while the results by RMF(DDDI) are closer to them, and the variation tendency is in accordance with them. Especially, at the magic number $N = 50$, the RMF(DDDI) result shows a large pairing gap as the experimental and the FRDM do, while the result of RMF(CPI) shows an opposite behavior. At $N = 82$, the same phenomenon appears although the experimental data is absent. The effect of the improvement of the DDDI is claimed therefore.

For proton pairing gaps, the accordance of the results of RMF(DDDI) with the experimental data and the results of FRDM is less pronounced, but is still better than those by RMF(CPI).

3.2 Total energy per nucleon

Figure 3 shows the total energy per nucleon (E/A) for Sr isotopes from the improved RMF(DDDI), RMF(CPI) and RMF, respectively. The known empirical values taken from the 1993 Atomic Mass Evaluation Tables [34] are also shown. The figure includes the prediction of FRDM [25] as well for comparison. Our calculated results by RMF(DDDI), RMF(CPI) and RMF are in agree-

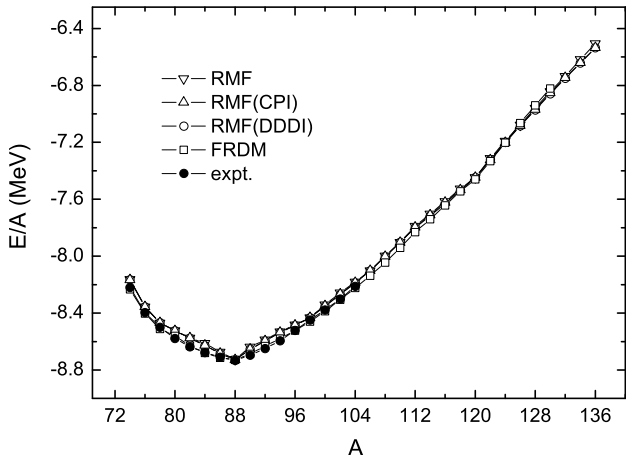

Fig. 3. The total energy per nucleon for the Sr isotope chain against the mass number A.

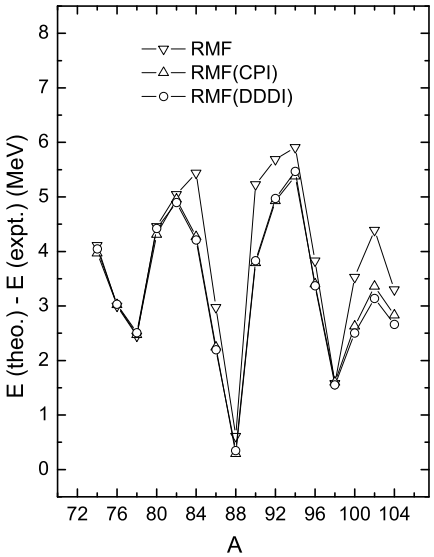

Fig. 4. The differences of the total energy between experimental data and different theoretical calculations (RMF, RMF(CPI) and RMF+BCS(DDDI)), respectively, for the Sr isotope chain.

ment with those from FRDM and experiment. All show parabolic shapes with a minimum total energy per nucleon being located at $A = 88$, where the neutron number $N = 50$ is a magic number. The total energies per nucleon by the RMF(DDDI) theory are in accord with the known empirical values in almost all the isotopes with deviations about 0.2 percent, only a few of them are closer to 0.5 percent. In order to show the effect of the RMF(DDDI) calculations, in fig. 4 the differences of the total energy per nucleon between the experimental data and three theoretical calculations, respectively, are shown. One can find that the RMF(DDDI) calculations give a better description of the total energy per nucleon than the other two calculations do, especially on the neutron-rich side.

3.3 Quadrupole deformation and shape coexistence

We have performed calculations in the RMF(DDDI), RMF(CPI) and RMF theory for both the prolate and oblate configurations. The deformations of nuclei have been obtained from the relativistic Hartree minimization with pairing. In fig. 5 we show the quadrupole deformation β_2 for the shape corresponding to the lowest energy. The predictions of FRDM [25] and known experimental values are also shown for comparison. It is seen that the RMF(DDDI) theory gives a well-defined prolate shape for lighter isotopes. Further, the addition of a few neutrons below the closed neutron shell leads to an oblate shape. This shape turns into a spherical one as the nuclei approach the magic neutron number $N = 50$. Nuclei above this magic number revert again to the prolate shape in the RMF(DDDI) theory. Then, a shape sequence from prolate-oblate-spherical-prolate is followed. It can be noticed that the RMF(DDDI), RMF(CPI) and RMF give nearly the same quadrupole deformations almost for all Sr isotopes. The three results are generally consistent with those from FRDM, and do not much deviate from the known experimental data.

In addition to the lowest minimum with prolate deformation, several isotopes exhibit a second minimum with

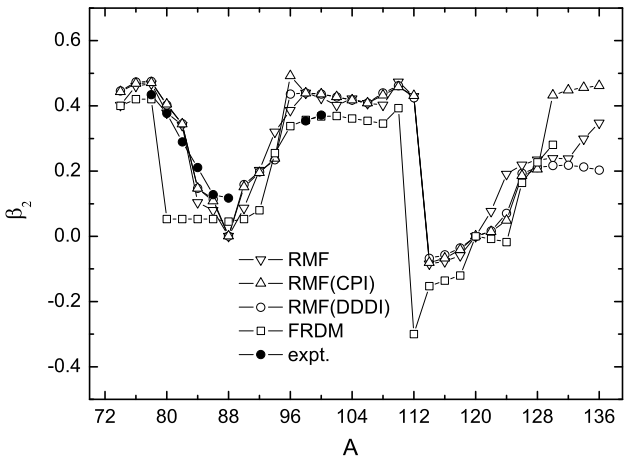

Fig. 5. The quadrupole deformation for the Sr chain against the mass number A.

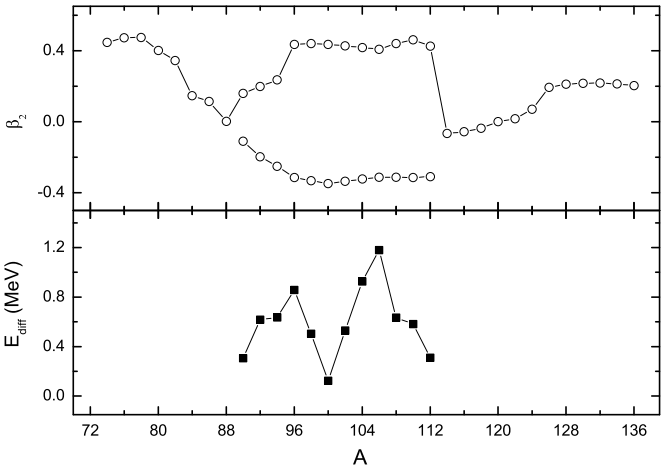

Fig. 6. Top: shape coexistence for Sr isotopes. Bottom: the energy difference is $E_{diff} = E_{oblate} - E_{prolate}$.

oblate deformation, the prolate and the oblate shapes differ in the total energy only by several hundreds keV, which may imply a shape coexistence. This is indicated in the upper part of fig. 6. The difference of the total ground-state energy between those of the oblate and prolate configurations is shown in the lower part of fig. 6. It shows that the Sr isotopes from $A = 90$ prefer prolate shapes. For nuclei close to $A = 112$, the total energy of nuclei with a prolate shape is only by about 300 keV larger than that of nuclei with an oblate shape.

3.4 Isotope shift

In fig. 7(a), the isotope shifts $r_c^2(A) - r_c^2(^{88}\mathrm{Sr})$ for the Sr isotope chain obtained from RMF+BCS(DDDI), RMF(CPI) as well as from RMF, are plotted as a function of the mass number A, with the semimagic nucleus ^{88}Sr serving as a reference nucleus. With increasing mass number A, the isotope shift changes only slightly until it reaches the magic number $N = 50$. Beyond the magic number it increases rapidly with mass number A. Such an anomalous behavior is a generic feature of deformed nuclei which usually appears in almost all isotopic chains in the rare-earth region [7,35–37]. The experimental data for Sr nuclei, indicated in the figure, exhibit a kink about the magic neutron number $N = 50$ [36], and the RMF(DDDI) theory and also the deformed RMF calculations are successful in reproducing this kink. This is because in the RMF calculations the isospin dependence of the spin-orbit term is well described, so that the level sequence of nuclei is reasonably reproduced, and which results in the correct nucleon distribution in the nucleus, implying that the kink has a minor dependence on the pairing correction. Nevertheless, the results from RMF(DDDI) and RMF(CPI) are closer to the experimental data than those from the deformed RMF without considering the pairing.

In order to obtain more information about this isotope shifts, the rms radii of the charge and neutron distributions of the Sr nuclei obtained with the RMF(DDDI)

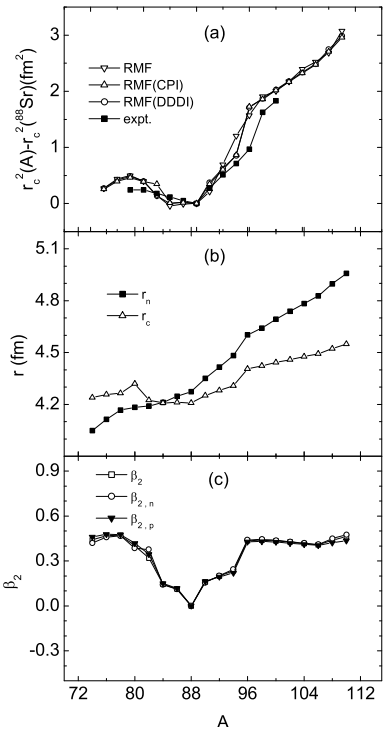

Fig. 7. Isotope shifts for Sr isotopes.

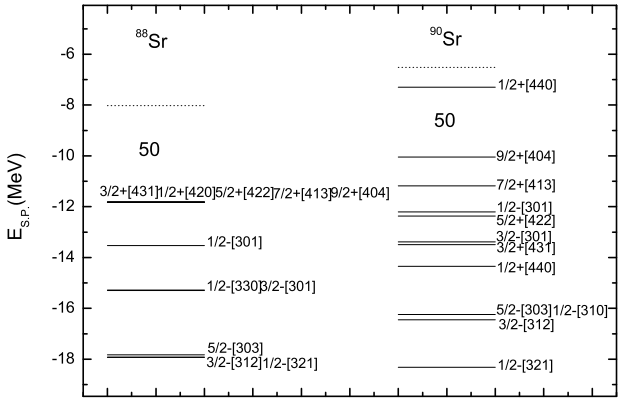

Fig. 8. Neutron single-particle energy levels of ^{88}Sr (left) and ^{90}Sr (right). The occupation probability of the states is presented by the length of the solid horizontal bars, and the scale of the obscissa measures the length of the bar. Dotted lines stand for the Fermi energies.

are presented in fig. 7(b), respectively. By going from the lighter isotopes to the heavier ones it is seen that the radius of neutrons increases with the mass number A. The increasing slope turns bigger at $N = 50$. The change of the slope can be explained by fig. 8, where the single-particle energy levels of ^{88}Sr and ^{90}Sr are plotted, and there the dotted lines stand for the Fermi levels for the two nuclei, respectively. The nucleus ^{88}Sr is a nearly spherical nucleus with several degenerate levels. The last degenerated level is at the energy -11.8 MeV, and there are 10 neutrons at this level. The levels in the nucleus ^{90}Sr are well separated, and the last two neutrons are distributed at the level $1/2^+[440]$ with an energy being equal to -7.3 MeV, which apparently will increase the radius of the nucleus ^{90}Sr in contrast to the radius of the nucleus ^{88}Sr. In addition, the neutrons distributed in $9/2^+[404]$ and $7/2^+[413]$ in ^{90}Sr with a higher energy than that of the degenerated level in ^{88}Sr will also increase the nuclear radius. The radius of protons basically does not change before $N = 50$, and after this point increases with A in spite of the fixed proton number in the chain. The close connection between the neutron and proton spatial distributions results from the self-consistent treatment of the strong pn attraction in the particle-hole channel. This can be further verified by fig. 7(c), where the quadrupole deformations for the neutrons and protons, as well as the nuclear matter, are shown. One may find that the deformation of protons follows the deformation of neutrons, although the proton number is constant, implying that the distribution of the protons is affected by the distribution of the neutrons in the nucleus.

3.5 Two-neutron separation energy

The two-neutron separation energy, S_{2n}, defined as

$$S_{2n}(Z,N) = B(Z,N) - B(Z,N-2), \qquad (22)$$

is quite a sensitive quantity to test a microscopic theory, where $B(Z,N)$ is the binding energy of nuclei with proton number Z and neutron number N. The two-neutron separation energy becomes negative when the nucleus is unstable against the two-neutron emission. In fig. 9, the two-neutron separation energies for Sr isotopes by RMF(DDDI) are plotted. The results of the RMF(CPI) and RMF calculations, the results of the FRDM [25] and the available experimental data [34] are also shown. Basically good agreement between experiment and the present calculation is found. The neutron shell closures at $N = 50$ and $N = 82$ can be clearly seen, so that the strong variation in the experimental separation energy at the neutron magic number $N = 50$ is well accounted for by the present

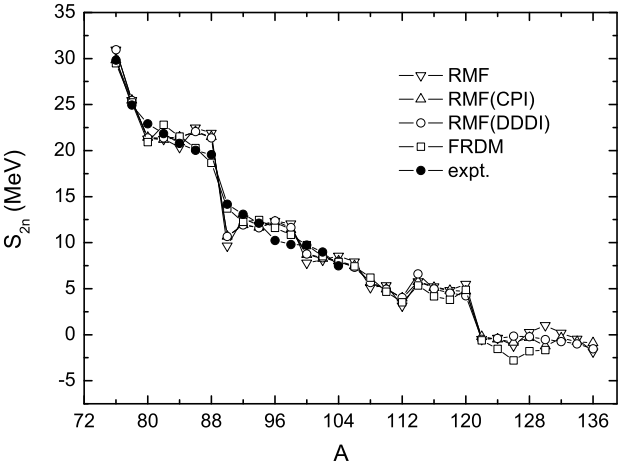

Fig. 9. Two-neutron separation energy for Sr isotopes.

Table 1. Partial contributions to the binding energy (in MeV). E_{part} is the energy of the particles (the sum of the single-particle energies, which already contains the interaction with the fields). E_σ is the contribution of the σ field (linear part), $E_{\sigma NL}$ the contribution of the σ field (nonlinear part), E_ω the contribution of the ω field, E_ρ the contribution of the ρ field, E_c the contribution of the Coulomb field, and E_{pair} the pairing energy. E_{CM} is the center-of-mass correlation. E is the total energy and E/A the total energy per nucleon.

	RMF				RMF+BCS			
	^{88}Sr	^{100}Sr	^{114}Sr	^{122}Sr	^{88}Sr	^{100}Sr	^{114}Sr	^{122}Sr
E_{part}	−2252.076	−2514.215	−2718.388	−2846.271	−2252.076	−2520.353	−2704.745	−2843.651
E_σ	12594.448	13962.038	15119.615	15918.960	12594.749	14007.869	15043.071	15906.648
$E_{\sigma NL}$	−238.462	−265.566	−292.721	−310.671	−238.467	−266.852	−292.189	−310.528
E_ω	−10611.118	−11727.403	−12645.525	−13271.956	−10611.418	−11764.178	−12578.317	−13261.037
E_ρ	−17.845	−55.287	−113.226	−156.523	−17.846	−56.143	−114.189	−156.273
E_c	−235.884	−227.024	−221.582	−219.574	−235.886	−226.896	−222.518	−219.512
E_{pair}	0.000	0.000	0.000	0.000	−0.0002	−1.571	−3.958	−2.242
E_{CM}	−6.913	−6.625	−6.342	−6.200	−6.913	−6.625	−6.342	−6.200
E	−767.852	−834.085	−878.169	−892.235	−767.857	−834.750	−879.185	−892.793
E/A	−8.726	−8.341	−7.703	−7.313	−8.726	−8.347	−7.712	−7.318

calculation. Furthermore, the two-neutron separation energy for the nucleus $A = 120$ is positive, while that for the nucleus $A = 122$ negative. Therefore the nucleus ^{120}Sr is predicted to be the last stable nucleus against two-neutron emission, *i.e.*, the neutron drip line nucleus. We will study their structure in sect. 3.7.

3.6 The partial contributions to the binding energy

In order to study the roles of the various mesons, photon, as well as pairing effect in the RMF approach, we list in table 1 the partial contributions to the binding energies of ^{88}Sr, ^{100}Sr, ^{114}Sr, and ^{122}Sr using RMF and RMF+BCS (DDDI), respectively. The E_{part}, which is the sum of the single-particle energies, already takes into account significant contributions from these field. From table 1, a remarkably balanced cancellation is observed between the σ and ω contributions (E_σ and E_ω). That is to say, the small nuclear binding energy arises from a cancellation between the large Lorentz scalar and vector potentials, each of which is comparable to the nuclear mass. It is necessary to study the ordinary nuclear systems in the relativistic framework to maintain the Lorentz transformation properties of the interaction. This leads naturally to various momentum-, density-, and spin-dependent effects. One may see that the nonlinear σ field is indeed important and $E_{\sigma NL}$ increases with the mass number A. This is consistent with the observation of Boguta and Bodmer [26], where the authors advocate the inclusion of these nonlinear terms for a better description, especially of the surface. The isospin dependence of the nuclear interaction is provided by the isovector ρ-meson, an increasing trend of E_ρ with mass number A can be observed. The pairing contributions to the binding energy are small, but they are nevertheless important for nonclosed-shell nuclei, resulting in the required partial occupancies of the single-particle levels. Comparing the single-particle energies E_{part} of the nuclei ^{88}Sr and ^{100}Sr obtained from the RMF+BCS(DDDI) calculation and those from RMF, one may find that the absolute value of E_{part}(RMF+BCS(DDDI)) is larger than that of E_{part}(RMF). It may be concluded that the nucleons in the nuclei ^{88}Sr and ^{100}Sr are more tightly bound by the pairing effect. However, in the nuclei ^{114}Sr and ^{122}Sr the results are opposite. The reason is that the nucleons of these nuclei are distributed with larger occupation probabilities at levels above the Fermi surface.

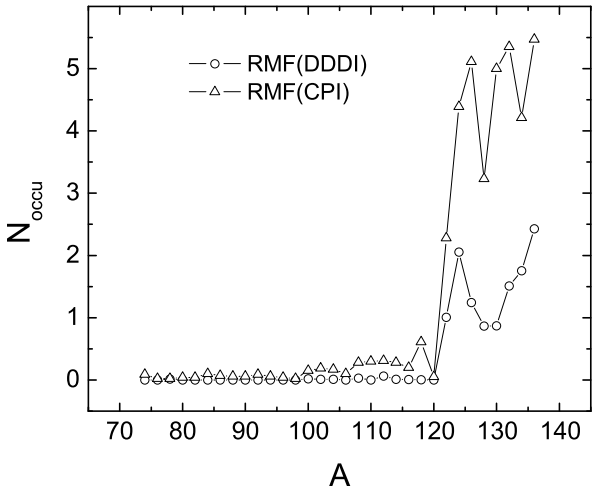

Fig. 10. The nucleon occupation numbers N_{occu} in the positive-energy states for Sr nuclei.

3.7 The effect of the DDDI pairing treatment

One interesting feature of exotic nuclei is the coupling to the continuum due to the pairing correlations. In this context, we studied the continuum levels and the particle oc-

Table 2. The comparison of the total energy, deformation, pairing energy between the calculated results by using 12 major harmonic-oscillator shells and 20 major harmonic-oscillator shells.

	Total energy		β_2		Pairing energy	
Major shells	12	20	12	20	12	20
^{122}Sr	−892.79	−896.03	−0.05	0.00	−2.24	−11.17
^{120}Sr	−893.65	−893.09	0.00	0.00	0.00	0.00
^{118}Sr	−888.57	−888.13	0.05	0.05	−0.88	−0.82
^{116}Sr	−883.96	−883.58	0.14	0.14	−1.537	−1.41
^{114}Sr	−878.51	−878.19	0.16	0.16	−2.49	−2.37

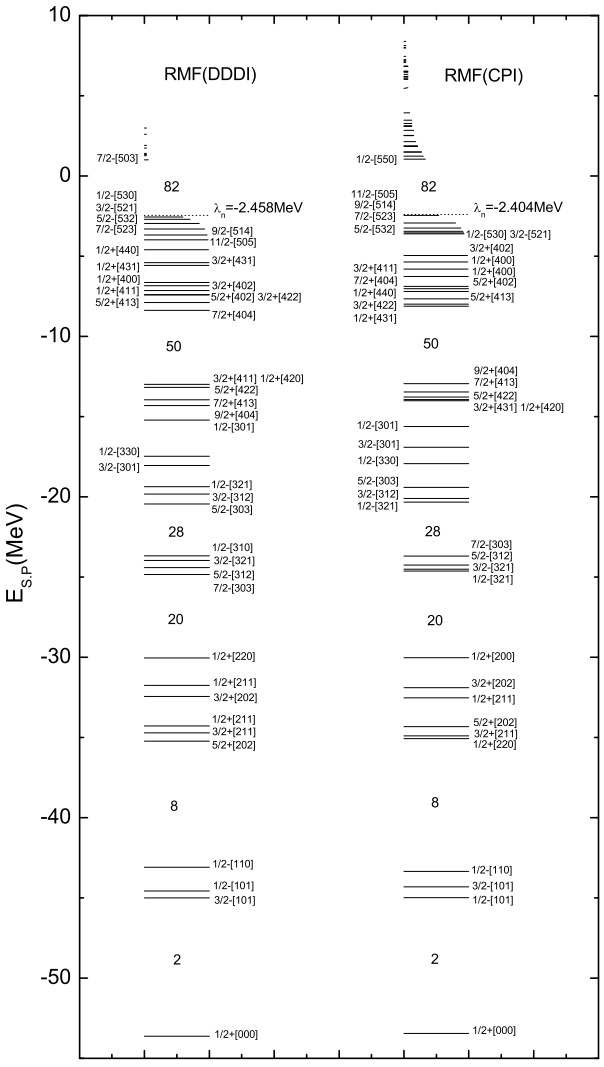

Fig. 11. Single-particle energy levels of ^{118}Sr. The dotted horizontal line represents the Fermi energy. In both panels, the occupation probabilities above the Fermi energy are multiplied by a factor of 30 for clarity.

cupation probabilities on the levels by using the constant pairing interaction (CPI) and the DDDI, respectively. The nucleon occupation numbers N_{occu} in the positive-energy states for Sr are plotted in fig. 10. It is seen that the nucleon occupation numbers N_{occu} in the positive-energy states by the CPI are generally larger than those by the DDDI, especially for nuclei $A > 120$. For the nucleus ^{120}Sr, the neutron number is 82, the magic number. It has been discussed before that ^{120}Sr is the last stable nucleus against two-neutron emission. When $A > 120$ in both cases, the N_{occu} increase steeply, which may indicate the failure of the BCS theory. This can be further depicted in fig. 11. In fig. 11, the neutron single-particle levels of the nucleus ^{118}Sr are plotted, with the length of the line proportional to the occupation probability of the neutron, which is from 0 to 2. The occupation probability shown in the positive region is amplified by 30 times for clarity. The level diagrams are calculated by DDDI (left) and CPI (right), respectively. The single-particle levels are labeled by the Nilsson quantum number. The pairing strengths, G_p and G_n, for protons and neutrons in the CPI are readjusted in order to obtain the same total energies as those obtained by the RMF(DDDI) for Sr isotopes. The single-particle levels from RMF with the CPI and with the DDDI below the Fermi surface are very similar and all magic neutron numbers at $N = 82$ and below are reproduced in the two cases, which implies that the pairing effect is mostly the surface effect. In fig. 11, although there are neutrons distributed at the positive-energy levels in both cases, the neutron occupation number in the DDDI calculation is much smaller than that in the CPI. In addition, the continuum states with bigger neutron occupation probabilities in the DDDI calculations are closer to the Fermi energy level, and so more localized in the nuclear region. Only a few levels with very small neutron occupation numbers appear at the higher-energy region. In contrast, the calculation with the CPI shows more continuum states with certain amount of neutron occupation probabilities in the higher-energy region, and these states seem to be unphysical. This sheds light on the evidence that the DDDI may have improved the BCS calculation for exotic nuclei.

In order to show the validity of BCS calculations in this work the convergence with respect to the number of oscillator shells has been checked. Besides the major shell $N_f = N_b = 12$, the $N_f = N_b = 20$ was also used in the calculations, and the results are shown in table 2. It is clearly shown that the results with both 12 and 20 shells in nuclei with $A \leq 120$ are very close to each other. It indicates that the convergence is fully satisfied, where the occupation number in the continuum is zero or very small (see fig. 10). Indeed, beyond the nucleus with $A = 120$, the cal-

culations give different binding energies, deformations and pairing energies. Therefore our results beyond $A = 120$ are no longer valid.

4 Summary and conclusion

We have formulated the RMF theory with the axially symmetric deformation and the DDDI for the pairing correlation. Conventional calculations for deformed nuclei are carried out by using the expansion method in terms of the axially symmetric harmonic-oscillator wave function and using a constant pairing interaction in the BCS method. This method is, however, not applicable to the case of nuclei close to the neutron or proton drip lines, since the positive states in the continuum for such nuclei are important, and cannot be reasonably treated by the conventional BCS theory. In order to improve the BCS method in the RMF theory, we introduced a DDDI for the pairing correlation, where the interaction between different paired nucleons is state dependent, and the positive states, whose wave functions are concentrated in the nuclear region, also contribute to the pairing matrix elements. This results in more reasonable single-particle energy level distributions and nucleon occupations. The theory by DDDI is generated to be available to describe the properties of nuclei closer to the drip line, so that the DDDI improved the BCS with CPI for describing nuclei in the drip line region.

Under the RMF calculation with the improved BCS using DDDI, the calculated binding energies, quadrupole deformations, two-neutron separation energies, and radii for nuclei in the whole Sr isotope chain from the proton drip line to the neutron drip line are all in agreement with the predictions of FRDM, and with available experimental data. Since the present calculation gives better level distributions and nucleon occupations, the isotope shift of the Sr isotope chain agrees better with experimental data than in the case of the RMF calculation without pairing and the case of RMF(CPI). The partial contributions from various mesons, photon, Coulomb interaction, and pairing energy are studied, which give some information about the change of nuclear structure with increasing neutron number.

In conclusion, the BCS theory is a simple and commonly used method to deal with the pairing interaction. The use of the DDDI to the BCS method has provided us a possibility to take into account the effects of the positive continuum states and on this basis to study the energy level distributions, occupations and the ground-state properties in the RMF theory with deformation in a self-consistent way. This theory and the resulting calculations describe the properties of nuclei in the drip line region well. It would be interesting to compare our results with those of the Hartree-Bogoliubov calculations for these nuclei.

The work is supported by the National Natural Science Foundation of China under Grant Nos. 10505016, 10235020, 10235030, 10275094, 10075080 and by the Knowledge Innovation Project of the Chinese Academy of Sciences under Grant No. KJCX2-SW-N17. The financial support from DFG of Germany is also gratefully acknowledged.

References

1. B.D. Serot, J.D. Walecka, Adv. Nucl. Phys. **16**, 1 (1986).
2. P.G. Reinhard, Rep. Prog. Phys. **52**, 439 (1989).
3. B.D. Serot, Rep. Prog. Phys. **55**, 1855 (1992).
4. P. Ring, Prog. Part. Nucl. Phys. **37**, 193 (1996).
5. Baoqiu Chen, Zhongyu Ma, F. Gruemmer *et al.*, Phys. Lett. B **455**, 13 (1999).
6. Hualin Shi, Baoqiu Chen, Zhongyu Ma, Phys. Rev. C **52**, 144 (1995); Zhongyu Ma, Hualin Shi, Baoqiu Chen, Phys. Rev. C **50**, 3170 (1994); Baoqiu Chen, Zhongyu Ma, F. Gruemmer, S. Krewald, Chin. Phys. Lett. **15**, 636 (1998).
7. G.A. Lalazissis, M.M. Sharma, P. Ring *et al.*, Nucl. Phys. A **608**, 202 (1996).
8. S.K. Patra, Cheng-Li Wu, C.R. Praharag *et al.*, Nucl. Phys. A **651**, 117 (1999).
9. Z.Z. Ren, H. Toki, Nucl. Phys. A **689**, 691 (2001).
10. Hongfei Zhang, Junqing Li, Wei Zuo, Zhongyu Ma, Baoqiu Chen, Soojae Im, Phys. Rev. C **71**, 054312 (2005).
11. L.S. Geng, H. Toki, E.G. Zhao, J. Phys. G **32**, 573 (2006).
12. W.Z. Jiang, Z.Z. Ren, T.T. Wang, Y.L. Zhao, Z.Y. Zhu, Eur. Phys. J. A **25**, 29 (2005).
13. Junqing Li, Zhongyu Ma, Baoqiu Chen, Yong Zhou, Phys. Rev. C **65**, 064305 (2002).
14. J. Dobaczewski, W. Nazarewicz, T.R. Werner, J.F. Berger, C.R. Chinn, J. Dechargé, Phys. Rev. C **53**, 2809 (1996).
15. J. Meng, Nucl. Phys. A **635**, 3 (1998); J. Meng, P. Ring, Phys. Rev. Lett. **77**, 3963 (1996).
16. K.A. Brueckner, T. Soda, P.W. Anderson, P. Morel, Phys. Rev. **118**, 1142 (1960).
17. V.J. Emery, A.M. Sessler, Phys. Rev. **119**, 248 (1960).
18. I.M. Green, S.A. Moszkowski, Phys. Rev. **139**, B790 (1965).
19. L.S. Geng, H. Toki, S. Sugimoto, J. Meng, Prog. Theor. Phys. **110**, 921 (2003).
20. A.B. Migdal, *Theory of Finite Fermi Systems and Applications to Atomic Nuclei* (Interscience, New York, 1967).
21. Suk-Joon Lee, J. Fink, A.B. Balantekin, M.R. Strayer, A.S. Umar, P.-G. Reinhard, J.A. Maruhn, W. Greiner, Phys. Rev. Lett. **57**, 2916 (1986).
22. C.E. Price, G.E. Walker, Phys. Rev. C **36**, 354 (1987).
23. Y.K. Gambhir, P. Ring, A. Thimet, Ann. Phys. (N.Y.) **194**, 132 (1990).
24. N. Sandulescu, L.S. Geng, H. Toki, G.C. Hillhouse, Phys. Rev. C **68**, 054323 (2003).
25. P. Moeller, J.R. Nix *et al.*, At. Data Nucl. Data Tables **59**, 185 (1995); **66**, 131 (1997).
26. J. Boguta, A.R. Bodmer, Nucl. Phys. A **292**, 413 (1977).
27. P. Ring, Y.K. Gambhir, G.A. Lalazissis, Comput. Phys. Commun. **105**, 77 (1997).
28. M. Abramowitz, I.A. Stegun, *Handbook of Mathematical Functions* (Dover, New York, 1970).
29. A.M. Lane, *Nuclear Theory* (Benjamin, 1964).
30. P. Ring, P. Schuck, *The Nuclear Many-Body Problem* (Springer, 1980).
31. S.J. Krieger, P. Bonche, H. Flocard, P. Quentin, M.S. Weiss, Nucl. Phys. A **517**, 275 (1990).
32. M.M. Sharma, M.A. Nagarajan, P. Ring, Phys. Lett. B **312**, 377 (1993).

33. M. Bender, K. Rutz, P.-G. Reinhard, J.A. Maruhn, Eur. Phys. J. **8**, 59 (2000).
34. G. Audi, A.H. Wapstra, Nucl. Phys. A **565**, 1 (1993).
35. E.W. Otten, in *Nuclear Radii and Moments of Unstable Nuclei*, in *Treaties on Heavy-Ion Science*, edited by D.A. Bromley, Vol. **7** (Plenum, New York, 1988) p. 515.
36. F. Buchinger, E.B. Ramsay, E. Arnold, W. Neu, R. Neugart, K. Wendt, R.E. Silverans, P. Lievens, L. Vermeeren, D. Berdichevsky, R. Fleming, D.W.L. Sprung, G. Ulm, Phys. Rev. C **41**, 2883 (1990).
37. M.M. Sharma, G.A. Lalazissis, P. Ring, Phys. Lett. B **317**, 9 (1993).